USGS
science for a changing world

Prepared in cooperation with the National Aeronautics and Space Administration

Global Geologic Map of Europa

By Erin J. Leonard, D. Alex Patthoff, and David A. Senske

Pamphlet to accompany
Scientific Investigations Map 3513

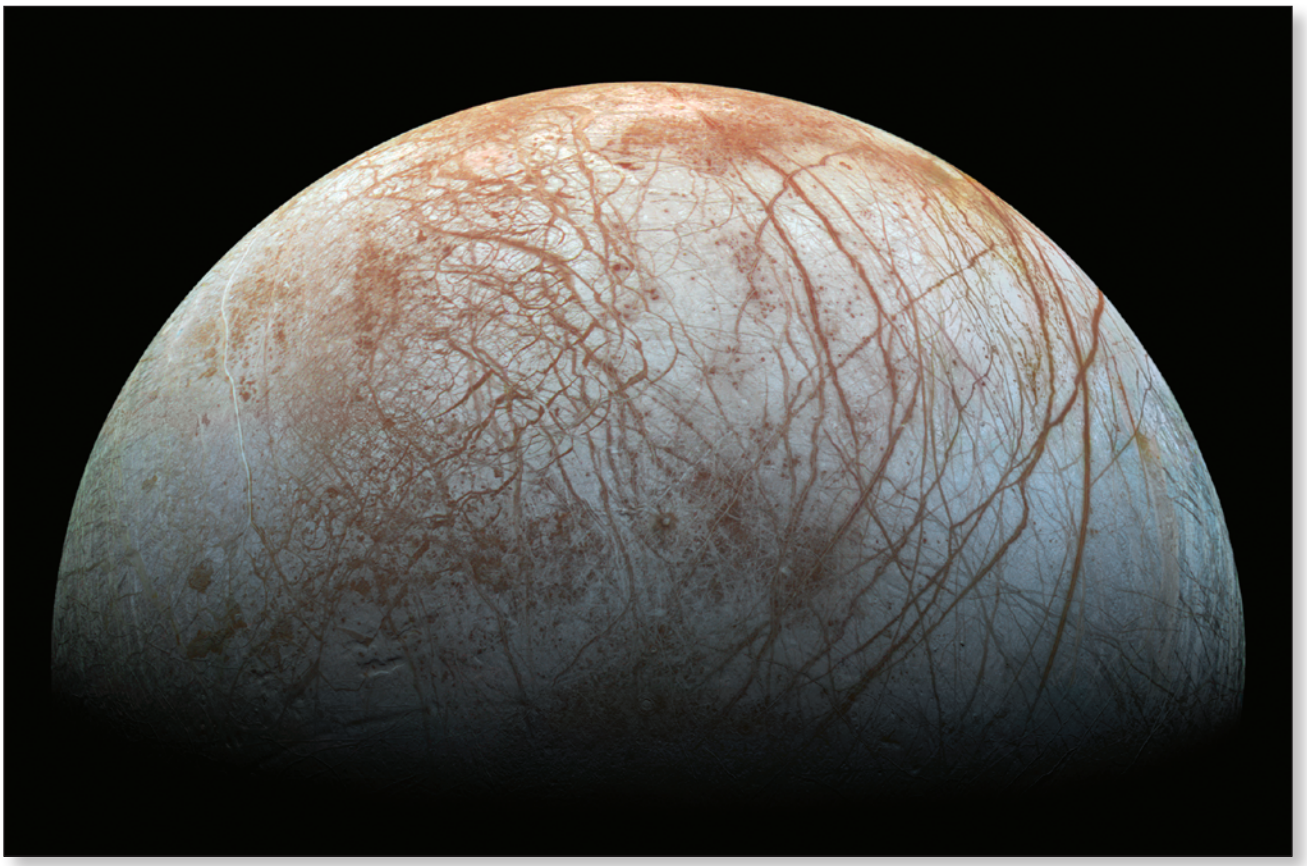

2024

U.S. Department of the Interior
U.S. Geological Survey

U.S. Geological Survey, Reston, Virginia: 2024

Suggested citation:
Leonard, E.J., Patthoff, D.A., and Senske, D.A, 2024, Global geologic map of Europa: U.S. Geological Survey Scientific Investigations Map 3513, scale 1:15,000,000, pamphlet 18 p., https://doi.org/10.3133/sim3513.

ISSN 2329-132X (online)
ISSN 2329-1311 (print)

Cover. Satellite image of Europa's anti-Jovian hemisphere. View is toward the north pole to the right and south pole to the left. Many dark cross-cutting bands and ridges of Falga Regio—particularly Minos, Cadmus, and Udaeus Lineae—can be seen on the right where they stand out starkly against the bright background of ridged plains. Near the middle, the impact crater Cilix features prominently near the terminator whereas the complex and curved bands of Argadnel Regio stretch toward the limb. Few arcuate depressions are seen on the left near the terminator with Thrace and Thera Maculae near where the bright band Agenor Linea stretches toward the limb. Images from NASA/JPL-Caltech/SETI Institute.

Contents

Figures

Tables

Global Geologic Map of Europa

By Erin J. Leonard,[1] D. Alex Patthoff,[2] and David A. Senske[1]

Introduction

Jupiter's moon, Europa, has been a source of intrigue since it was discovered by Galileo Galilei more than 400 years ago and imaged in detail by the Voyager 2 and Galileo spacecraft. A range of science investigations suggests that Europa contains the key ingredients for habitability—notably energy, chemistry, and liquid water (Wackett and others, 2004; Hand and others, 2009). Geologic maps of Earth and rocky planetary bodies typically consist of units that are primarily based on lithologic differences. When describing the geology of Europa, it is important to note that this geology is occurring in the solid ice crust, not rock. Geologic units identified on Europa are assumed to represent three-dimensional volumes of ice, each with a distinct relative brightness, texture, or unique structure. The actual depths of the units are unknown. Following the definition laid out by Wilhelms (1990) for geologic mapping of icy satellites, a new geologic unit is defined when the region is modified to the point that it no longer has its original properties. We specifically note and emphasize that the structural and morphologic differences between units could be due to a variety of factors, including compositional variation, tectonic deformation, or physical or chemical alteration or by some other endogenic or exogenic process.

Europa's surface is geologically complex and, based on the dearth of impact craters, is interpreted to be as young as ~60 Ma (Lucchitta and Soderblom, 1982; Pappalardo and others, 1999b; Bierhaus and others, 2001, 2009; Figueredo and Greeley, 2004; Prockter and Schenk, 2005; Doggett and others, 2009). The array of geologic features that characterize the surface include extensive regional plains; regions of broad disruption, termed chaotic terrain; long, quasi-linear ridges that span thousands of kilometers; and bands as wide as 60 kilometers (km) that extend for hundreds to thousands of kilometers (for example, Prockter and Patterson, 2009) (fig. 1, map sheet). These features, combined with other geophysical measurements (Kivelson and others, 2000), suggest the presence of a global, briny, liquid water ocean >100 km deep beneath an ice shell tens of kilometers thick (Cassen and others, 1979, 1982; Anderson and others, 1998; Pappalardo and others, 1999b; Kargel and others, 2000; Kivelson and others, 2000; Nimmo and Manga, 2009; Schubert and others, 2009; Vance and Goodman, 2009; Zolotov and Kargel, 2009). The arrival of the Galileo spacecraft in 1995 revealed the true nature and level of complexity of Europa's surface. Although image data returned by Galileo provided insight into the structure of a variety of regions, the entire satellite has yet to be observed at a consistent scale (image resolution ranges from 8 meters per pixel [m/px] to 20 kilometers per pixel [km/px]), and the detailed geologic nature of much of its icy surface remains a mystery. Establishing the global context of the distribution and timing of Europan geologic units forms a basis to understand regional- and local-scale processes, serves as a tool for the planning of future missions, and, most of all, is essential to gaining insight into the potential habitability of this icy world.

Following the general procedures of planetary mapping (Wilhelms, 1972, 1990; Greeley and Batson, 1990; Tanaka and others, 2011), we generated a global map of Europa at a scale of 1:15,000,000. We established four areally extensive primary material units that are divided into geologic subunits: (1) regional plains material (unit pr)—a high-relative-brightness material that is seemingly smooth at global resolution (>1 km/px); (2) band material (unit b)—linear to curvilinear zones, greater than 15 km in width, with a distinct, abrupt change in relative brightness from the surrounding region; (3) high-relative-brightness chaos material (unit chh), mottled chaos material (unit chm), low-relative-brightness chaos material (unit chl), and Moytura chaos material (unit chM)—various morphological types of chaos materials; and (4) crater material (unit c), continuous crater ejecta material (unit ce), Pwyll radial crater ejecta material (unit cpre), and Pwyll crater ray material (unit cpr)—materials associated with impact craters including their local deposits, farther ranging ejecta material, and central structure. We also identify structures that are too small areally to be distinguished at map scale but are significant enough to be mapped as line symbols: ridge linea, undifferentiated linea, band linea, high-relative-brightness band linea, cycloid, multi-ring structure, trough, and depression margin. Microchaos is defined as a disrupted terrain with variable textures and apparent relative brightness that ranges from high to low. An individual michrochaos is too small (5–25 km diameter) to be distinguished at the 1:15,000,000 map scale, but its presence is ubiquitous and significant enough to be identified on the map as point symbols. Small craters (5–10 km diameter) and central

[1]Jet Propulsion Laboratory, California Institute of Technology

[2]Planetary Science Institute

peak structures are two additional point features for structures associated with impact craters that are too small to map at the 1:15,000,000 map scale. This map provides a global stratigraphic framework for Europa as a basis for future quantitative assessment of the distribution of the various geologic terrains.

Background and Rationale

The earliest efforts to map Europa on a global scale were based on image data from the Voyager missions that were limited in spatial coverage by a resolution ranging from ~2 km/px to >20 km/px (Lucchitta and Soderblom, 1982). On the basis of this limited dataset, Lucchitta and Soderblom (1982) identified two major terrains—mottled terrain (brown and gray) and plains material (bright, dark, and fractured)—that were further subdivided based on color, relative brightness, and texture. Brown mottled-terrain materials were defined as uniformly hummocky in texture and darker than the gray mottled-terrain materials, which were coarser in texture. Bright plains and dark plains were defined based on relative brightness, which Lucchitta and Soderblom (1982) proposed to be caused by the effects of sputtering (lag deposits and frost) or small-scale features that could not be resolved at map scale. Fractured plains were defined by the presence of a regionally localized dense pattern of fractures. Structural-feature mapping was restricted to the largest lineations (dark wedge-shaped bands and triple bands), dark spots, ridges, and impact craters. Lucchitta and Soderblom (1982) concluded that the oldest terrain is likely the bright plains unit, followed by a mixture of gray mottled-terrain materials and dark plains, followed by the emplacement of brown material in mottled terrain or spots, and then by the formation of ridges. Although their map laid the foundation for future studies of the surface of Europa—identifying the two dominant surface terrains, the lack of impact craters, and numerous lineations—it was limited by the resolution of the data returned by the Voyager spacecraft.

Relative to the Voyager spacecraft, the Galileo mission (1997–2003) provided an improved image data set with resolutions as high as 8 m/px (Greeley and others, 2000). Lower resolution, ~1 to 2 km/px, image data covers a significant portion (~70 percent) of Europa's surface and helped to reveal the broad global character of this icy world (Doggett and others, 2009). Images at scales larger than 1 km/px (~10 percent of the surface) revealed numerous individual ridges, fractures, domes, and details of different terrains.

During the Galileo mission, Greeley and others (2000) outlined a set of guidelines for geologic mapping of Europa, identified units, defined a naming convention for features, and suggested a color scheme for map units. The four main geologic unit types include craters, chaoses, bands, and ridged plains. Craters incorporate impact-crater-related materials (to be denoted on Europa geologic maps in shades of orange and yellow). "Chaos," a new terrain relative to mapping from the Voyager data, consists of irregularly shaped slabs separated by intervening fine-textured matrix material (to be denoted on Europa geologic maps in shades of green). The linear features that crisscross the surface of Europa and typically appear to be composed of a dark material were named "bands" (to be denoted on Europa geologic maps in shades of purple). Finally, high-relative-brightness terrain, making up the majority of Europa's surface, contains a complex array of crosscutting ridges and troughs named "ridged plains" (to be denoted on Europa geologic maps in shades of blue). While the work of Greeley and others (2000) did not result in a published geologic map, subsequent geologic mapping has been based on this naming and coloring scheme.

Using the geologic mapping framework of Greeley and others (2000), Figueredo and Greeley (2000, 2004) produced geologic maps of regional scale (<250 m/px), north to south Galileo imaging transects located along the leading and trailing hemispheres of Europa (~10 percent of Europa's surface). This work subdivided chaos, bands, and plains into a refined set of units on the basis of texture. They further subdivided ridges and bands using inferred stratigraphic relations. Based on their results, Figueredo and Greeley (2004) found that Europa's surface history can be generally divided into four periods. The first period is dominated by the formation of ridged plains material that was followed by the emplacement of subdued ridged plains material. The second period was dominated by the formation of lineated, smooth, and ridged bands emplaced coevally with some of the ridges and ridge complexes. In addition, the formation of a subdued chaos unit took place during the second half of this period. The third period was dominated by the formation of chaos material and a few instances of pitted subdued plains. The fourth, and most recent, period was characterized by the formation of the young smooth bands, ridge complexes, and ridges emplaced coevally with a subunit of elevated chaos. The limited number of impact craters for absolute age dating and, therefore, the relatively few crosscutting relations with other units suggests that they were likely emplaced during the third and fourth period but in some places might date to the second period or earlier. The resurfacing history inferred by Figueredo and Greeley (2004) is similar to that suggested by Lucchitta and Soderblom (1982) but elucidates greater detail and refines the relation between chaos (mottled terrain) and the ridged plains (plains terrain). While these detailed maps provided insight into stratigraphic relations on a regional scale, they did not include a global framework in which to relate them to each other.

To understand the context for regional-scale mapping, a global framework is necessary. A preliminary global geologic map for Europa was produced by Doggett and others (2009). This mapping focused on identifying lineaments and units (plains material, ridge material, band material, chaos material, and crater units) on the leading and trailing hemispheres of Europa and follows the taxonomy presented by Greeley and others (2000). Expanding on previously established unit types, this work identified what they termed the "Argadnel Regio south unit" and the "lenticulated terrain unit." In addition, this analysis subdivided chaos into four variations on the basis of relative age inferred from relative brightness and color. Similar to previous work, Doggett and others (2009) inferred four periods of resurfacing, the first of which encompasses the formation of ridged plains and their chaos 1 unit. The second period is distinguished by the emplacement of the ridge unit and the Argadnel Regio south unit. This was followed by the formation of the western Powys Regio chaos, lenticulated terrain, and the chaos 3 units in the

third period. Lastly, the fourth period is characterized by the emplacement of the chaos 4 unit. Relative to the inferred history of Figueredo and Greeley (2004), Doggett and others (2009) inferred relative age through the subdivision of the chaos. While this map attempts to relate units across Europa globally, it only focuses on the areas imaged at a resolution <2 km/px with little attempt to bridge the resolution gaps on the sub-Jovian (facing towards Jupiter) and anti-Jovian (facing away from Jupiter) hemispheres. Thus, the full global analysis of geologic units across Europa's surface remained incomplete.

In addition to the regional and preliminary global-scale mapping, various theme or sketch maps have been published using Galileo Solid State Imaging (SSI) data, typically at higher resolution (<250 m/px). These investigations generally focused on specific terrain types or geologic processes and tend to not use a consistent set of units relative to each other. These regional- to local-scale studies advance our understanding of relative stratigraphic relations of individual features and classes of structures and allow for formation mechanisms to be refined (Head and others, 1998; Senske and others, 1998; Spaun and others, 1998a, b; Klemaszewski and others, 1999; Prockter and others, 1999; Sullivan and others, 1999; Williams and others, 1998; Kadel and others, 2000; Figueredo and others, 2002; Prockter and Schenk, 2002; Kattenhorn, 2002).

Our global geologic map of Europa (map sheet) strives to create a consistent and representative view of the entire surface of this icy world. Our approach allows for a holistic analysis of Europa and its terrains. The endeavor of generating a uniform global geologic map of Europa as a U.S. Geological Survey (USGS) product was initiated in the early 2000s by a team led by Professor Ron Greeley of Arizona State University. This task resulted in preliminary maps by Doggett and others (2009) and Bunte and others (2013), neither of which are available in a digital GIS format and the latter only being available as a conference abstract. With the passing of Professor Greeley in 2011, some remaining members of the team regrouped in 2015 and augmented the effort using the preliminary mapping as a foundation to complete the effort of generating a fully digital GIS global geologic map of Europa. Our map (map sheet) encompasses the current state of knowledge of Europa's geology, contains all original linework, and follows the taxonomy laid out in Greeley and others (2000) when defining the units. This resulting product is a tool for quantitative geologic analysis and serves as a foundation for planning observations for the Europa Clipper mission now under development.

Physiographic Setting

With relatively little topographic relief compared to other bodies in the solar system, the landmarks that define Europa's geography are coherent areas of brightness. We organize this geography by global hemispheres (sub-Jovian, anti-Jovian, leading, and trailing). The locations of the hemispheres are fixed because Europa is tidally locked to Jupiter, meaning the same side of Europa always faces Jupiter, similar to Earth's Moon. The "sub-Jovian hemisphere" is the half of Europa's surface that faces Jupiter and the "anti-Jovian hemisphere" is the half that never faces Jupiter. The leading and trailing hemispheres are defined by the direction of Europa's orbital movement where the "leading hemisphere" centers on the half of Europa facing the direction of motion and the "trailing hemisphere" faces away from the direction of motion. Dividing the moon by these four faces, each consisting of half the moon, results in overlaps. Instead, we divide Europa's surface into four quadrants with each defined by a portion of the two halves described above (fig. 1*A*): trailing sub-Jovian (long 0–90° E.), trailing anti-Jovian (long 90–180° E.), leading anti-Jovian (long 180–270° E.), and leading sub-Jovian (long 270–360° E.). The coordinate system used here, planetocentric positive east longitude (longitude reference point is the center of the crater Cilix, at 178° E.), is being used by the National Aeronautics and Space Administration (NASA) Europa Clipper and the European Space Agency (ESA) Jupiter Icy Moons Explorer (JUICE) missions (Phillips and Korth, 2017). We include descriptions of the four quadrants and a representative selection of features. All the features on Europa are named from Celtic mythology or the Greek myth of Europa (Doggett and others, 2009). For a full list of named geographic features or regions on Europa, see the International Astronomical Union Gazetteer of Planetary Nomenclature (https://planetarynames.wr.usgs.gov/).

Europa's surface mostly consists of terrains, or regiones (singular, regio), that have either a comparatively uniform relative high brightness or a low relative brightness that can appear mottled. Europa's "high-relative-brightness terrains" appear blue-white in corrected true color images taken by the Galileo spacecraft (Greeley and others, 2000). This terrain is mostly composed of water ice and a relatively small non-ice component (Dalton and others, 2012). The named high-relative-brightness terrains are Balgatan Regio and Falga Regio. Europa's low-relative-brightness or mottled terrains appear orange-brown in corrected true color images taken by Galileo (Greeley and others, 2000). This color variation is thought to result from its unique composition and possibly radiation processing of the surface materials. The composition of the low-relative-brightness terrain is thought to be dominated by magnesium sulfate ($MgSO_4$) (McCord and others, 1999) or sodium chloride (NaCl) (Trumbo and others, 2019). The radiation environment imposed by Jupiter at Europa's orbit results in high-energy particles (~1–50 million electron volts [MeV]) bombarding the surface and, therefore, processing and altering the surface material (for example, Cooper and others, 2001). Additionally, sulfur ions ejected from Io are hypothesized to impact Europa, primarily on the trailing hemisphere (Dalton and others, 2013), which can result in surface-color variations. Europa's named low-relative-brightness terrains are Annwn Regio, Moytura Regio, Dyfed Regio, Powys Regio, and Tara Regio.

The other prominent terrains on Europa are the lineae, maculae, and ringed features. Numerous lineae or linear features, long but narrow stretches of terrain, crisscross Europa's surface, giving it a ball-of-string appearance (Pappalardo and others, 1999a). This linear- to curvilinear-shaped terrain can be high or low relative brightness, which could indicate a difference in composition (for example, Prockter and others, 2017) with respect to the background terrain. Numerous named lineae are visible on Europa's surface; some of the most prominent

include Udaeus Linea, Minos Linea, Cadmus Linea, Euphemus Linea, and Agenor Linea. These lineae typically span multiple quadrants but are noted below in the quadrant where the linea is predominately present. A subtype of linea, "flexus," henceforth referred to as "cycloids" due to the prominent use in the Europa literature (for example, Hoppa and others, 1999; Kattenhorn and Hurford, 2009; Rhoden and others, 2021), are lineae made up of a series of arcuate lineae connected by sharp cusps. "Maculae" are quasi-circular spots or terrain with a brightness difference (typically lower) compared to the surrounding terrain. As opposed to some of the low-relative-brightness regiones, maculae are smaller in areal extent and include Castalia Macula, Thrace Macula, and Thera Macula. Two known large ringed features on Europa—Tyre (62 km diameter[1]) and Callanish (23 km diameter)—are terrains commonly hypothesized to be remnants of impacts that penetrated the ice shell (Moore and others, 1998; Schenk, 2002) and are somewhat similar in morphology to Tegid crater (22 km diameter).

Trailing Sub-Jovian Quadrant (Longitude 0–90° E.)

The trailing sub-Jovian quadrant is characterized by a variety of terrains but is dominated by Annwn Regio and Moytura Regio. Annwn Regio is a mottled low-relative-brightness terrain approximately centered about the equator, generally extending from lat ~30° S. to ~40° N. and from long ~350° E. to ~80° E. A portion of Balgatan Regio, located in the southwestern region of this quadrant, is a high-relative-brightness terrain with few crisscrossing dark lineaments. To the east of Annwn Regio lies Conamara Chaos, a type example for low-relative-brightness chaos material containing low-relative-brightness matrix material and rounded blocks of regional plains material. Moytura Regio, located in the extreme southwest, is the type example for Moytura chaos material (see Description of Map Units, map sheet).

This quadrant also contains arguably the most prominent crater on Europa's surface, Pwyll crater (lat 25° S., long 89° E.; 47 km diameter), because its bright rays emanate for thousands of kilometers away from the central impact point. No other craters with obvious rays are visible on Europa's surface, despite the existence of other craters of similar size; Moore and others (1998) hypothesized that radiation processing has caused older rays to fade. For this reason, Schenk and Turtle (2009) interpreted Pwyll crater to be one of the youngest craters on Europa. The large ringed feature, Callanish (lat 16° S., long 26° E.; 23 km diameter), is interpreted to be one of three craters on Europa's surface with visible basin rings. Its morphology suggests that the impact penetrated Europa's ice-shell (Moore and others, 1998; Schenk, 2002).

[1]The crater diameters identified in this map are based on the diameter of the crater material unit (c), which could encompass the diameter of the crater rim and some of the surrounding material, because the crater-rim structure is not identifiable at the basemap resolution. Thus, the diameter values in this map text may differ from the diameters cited in other works (for example, Schenk and Turtle, 2009), where high-resolution images that are not included in the basemap for this work reveal the structure of the crater rim.

Trailing Anti-Jovian Quadrant (Longitude 90–180° E.)

The trailing anti-Jovian quadrant is dominated by Dyfed Regio, Argadnel Regio, and Falga Regio. Having a mottled low-relative-brightness, Dyfed Regio, extends from lat 20° S. to ~30° N. and from long 100° E. to ~130° E. Immediately to the east of Dyfed Regio is Castalia Macula (lat 2° S., long 134° E.), a landform containing two mesas surrounded by a smooth, dark terrain that Prockter and Schenk (2005) find to have the largest topographic relief on Europa (~2 km). Also located around the equatorial region of this quadrant (between Dyfed and Powys Regiones to the east) is the unique terrain of Argadnel Regio, which consists of arcuate to circular bands of low-relative-brightness material (Prockter and others, 1999). Directly to the north of Argadnel Regio is the high-relative-brightness terrain of Falga Regio. Greeley and others (2000) identified Falga Regio as the type example of their ridged plains material (here identified as regional plains material), because it exhibits a multitude of crisscrossing lineaments, such as Udaeus Linea, Minos Linea, and Cadmus Linea. South of Argadnel Regio lies Agenor Linea, a prominent and unique very high-relative-brightness lineament. Geissler and others (1998) suggested that the unusual brightness of this feature may be due to the effect of the grain size of material making up the central part of this linea.

Leading Anti-Jovian Quadrant (Longitude 180–270° E.)

The named regiones, Powys Regio and the western part of Tara Regio, in the leading anti-Jovian quadrant are concentrated in the equatorial region and are generally smaller than those in the quadrants to the west. Powys Regio is a mottled low-relative-brightness terrain extending from lat ~35° S. to ~20° N. and from long ~190° E. to ~245° E. Similarly, the western part of Tara Regio (lat ~5° N. to ~30° S. and long ~240° to 270° E.) is a mottled low-relative-brightness terrain. Located to the southwest of Powys Regio and on the border between the trailing anti-Jovian and leading anti-Jovian quadrants are Thrace Macula (lat 46° S., long 188° E.) and Thera Macula (lat 44° S., long 178° E.) that are among the darkest features on Europa's surface. Directly to the north of Powys Regio is Tyre, another prominent ringed feature that is hypothesized to be an impact structure that penetrated Europa's ice shell (Moore and others, 1998; Schenk, 2002).

Leading Sub-Jovian Quadrant (Longitude 270–360° E.)

The leading sub-Jovian quadrant is dominated by the eastern part of Tara Regio and the expansive area of Balgatan Regio. Tara Regio is a mottled low-relative-brightness terrain that extends from lat ~40° S. to ~20° N. and from long 260° to 310° E. Adjacent to Tara Regio is Murias Chaos (lat 22° N., long 276° E.), which is designated as the type locality of high-relative-brightness chaos material consisting of high-relative-brightness material with angular blocks of regional

plains material. Along the east edge of the quadrant (long ~350° E.) lies a portion of Annwn Regio that extends into the trailing sub-Jovian quadrant. To the south of Tara Regio and Annwn Regio is the westernmost part of Balgatan Regio, a high-relative-brightness terrain. This portion of Balgatan Regio contains numerous cycloids (see Cycloid section), and other dominant lineae, such as the prominent Euphemus Linea.

Mission Data and Base Map

The suite of images used for our geologic mapping combines data sets obtained from both the Voyager and Galileo missions. The Voyager 1 and 2 spacecraft imaged Europa during flybys in March and July 1979, respectively. The Voyager 1 global images ranged in resolution from 30 to 100 km/line pair (lp), or minimum distance between two resolvable features, while Voyager 2 provided multispectral (300–650 nanometer [nm]) (Smith and others, 1977) coverage of ~20 percent of the surface with resolutions as high as 2–4.5 km/lp over the area between long ~130° and ~210°. The Galileo mission made 12 flybys (out of a total 21 flybys of all four Galilean satellites) of Europa between June 1996 and January 2002 and acquired images primarily of the anti-Jovian hemisphere (between long ~135° and 225° E). Relatively high-resolution imaging (<250 m/px) was possible during each targeted flyby covering ~1 percent of the surface (Doggett and others, 2009). Ultimately, approximately 36 percent of the surface was imaged at 1 km/px or larger by the Galileo mission. Most of the remainder of Europa was imaged at a lower resolution that was adequate for the 1:15,000,000 map scale. However, two areas near the poles remain where no image data is available. These areas are white to denote no data. Figure 2 (map sheet) shows the distribution of coverage resolution from both Voyager and Galileo image data used to create the base map mosaic. The multiple-flyby nature of the Galileo mission resulted in viewing and lighting geometries that varied significantly (fig. 2). This variation is generally common for spacecraft observations of the outer-planet satellites and must be considered when mapping, because some regions are dominated by changes in brightness while others are dominated by topographic shadowing. While this range of emission and incidence angles allows for characterization of morphology and photometric properties, it must be carefully considered when determining surface geology. The Methodology section elaborates on the methods we used to maintain consistency in the unit definition across various emission and incidence angles.

The cartographic base for this geologic map is a controlled photomosaic of Europa (fig. 1*A*; U.S. Geological Survey, 2002), which combined the highest quality images of moderate resolution generated by the Galileo Solid State Imager (SSI) and the Voyager 1 and 2 cameras (Batson, 1987; Becker and others, 1998, 1999, 2001). Because of the failure of Galileo's high-gain antenna to deploy fully, the highest-resolution imaging (tens of meters per pixel) was limited to a number of dominant terrain and feature types. Consequently, Voyager data remains the highest-resolution coverage of some areas, for example, the strip centered near 150° E. The global digital image map was produced using Integrated Software for Imagers and Spectrometers (ISIS2) (Eliason, 1997; Gaddis and others, 1997; Torson and Becker, 1997). Individual images were radiometrically calibrated and photometrically normalized using a lunar-Lambert function with empirically derived values (McEwen, 1991; Kirk and others, 2000). A linear correction based on the statistics of all overlapping areas was then applied to minimize image brightness variations. Although consistency was achieved where possible, different filters were included for global image coverage as necessary: the clear filter (centered on 497 nm) and blue filter (centered on 470 nm) for Voyager 1 and 2 (Smith and others, 1977; Danielson and others, 1981); clear filter for (380 –1,050 nm) near-IR (757 nm); and green (559 nm) filters for Galileo SSI (Belton and others, 1992). The process of creating a geometric control network began with selecting control points on the individual images, making pixel measurements of their locations using reseau locations (a grid of black dots on the images used as a reference marking) to correct for geometric distortions (Voyager) and converting the measurements to millimeters in the focal plane. These data were combined with the camera focal lengths and navigation solutions as input to a photogrammetric triangulation solution (Davies and others, 1995, 1998; Davies and Katayama, 1981).

During the creation of the USGS global mosaic (U.S. Geological Survey, 2002), a compromise of 500 m/px resolution was used, because many of the higher resolution images were down-sampled and lower resolution data were up-sampled in an attempt to create a consistent portrayal of observable features. Moreover, only images of moderate emission or incidence angles were used to reduce contrast differences between the images. The final constructed sinusoidal-projection mosaic was then reprojected to Mercator and polar stereographic projections for latitudes below and above 57°, respectively (fig. 1*A*).

Mapping on the anti-Jovian hemisphere was supplemented with an image mosaic (fig. 1*B*) that includes almost all images with pixel scales between 165 m and 1 km obtained by Galileo in the region from lat 83.5° N. to 72.5° S., long 70° to 201.5° E. The entire mosaic was sampled to the resolution of the best available image, at a pixel scale of 165 m. Mosaic processing began by tying features in several lower resolution background images to their geographic coordinates in the USGS global image mosaic (sampled at 500 m/px). The background images used to tie the 72 higher resolution images can be found in table 1. For this map, this mosaic was used to aid in unit identification only, not as a base map.

Methodology

We set the scale for this geologic map at 1:15,000,000 to capture enough detail to delineate major units and identify prominent linear features on Europa while also fitting on a single map sheet. We drafted all the linework using GIS software at a digital scale of 1:4,000,000 and used a vertex spacing of 4 km. At this mapping scale, we identify units and lineae that are of sufficient aerial extent or prominence (see Units and Linear Features sections) to represent the global geology despite the varying resolution of the base map. The linework was slightly smoothed for aesthetics.

Table 1. Image numbers, resolution, and incidence angles of each image in the image mosaic of Europa.

[Figure 1 shows image mosaic of Europa, and the U.S. Geological Survey global image mosaic is available at https://astrogeology.usgs.gov/search/map/Europa/Voyager-Galileo/Europa_Voyager_GalileoSSI_global_mosaic_500m. km, kilometer; m, meter]

Image number	Resolution	Incidence angle
Background		
G1ESGLOBAL01_03498751.13	1.6 km	38°
G1ESGLOBAL01_03498751.26		
G1ESGLOBAL01_03498751.39		
G1ESGLOBAL01_03498751.78		
14ESGLOCOL01_04409848.65	1.45 km	75°
14ESGLOCOL01_04409849.00		
14ESGLOCOL01_04409849.26		
Higher resolution images		
11ESREGMAP01_04206192.00	220 m	75°
11ESREGMAP01_04206192.13		
11ESREGMAP01_04206192.26		
11ESREGMAP01_04206192.39		
11ESREGMAP01_04206192.52		
11ESREGMAP01_04206192.6		
11ESREGMAP01_04206192.78		
11ESREGMAP01_04206193.00		
11ESREGMAP01_04206193.13		
11ESREGMAP01_04206193.26		
14ESWEDGES01_04409551.65	230 m	39°
14ESWEDGES01_04409551.78		
14ESWEDGES01_04409552.00		
14ESWEDGES01_04409552.13		
14ESWEDGES01_04409552.26		
14ESWEDGES01_04409552.39		
14ESWEDGES01_04409552.52		
14ESWEDGES01_04409552.65		
14ESWEDGES01_04409552.78		
14ESWEDGES01_04409553.00		
15ESREGMAP01_04499618.00	228 m	81°
15ESREGMAP01_04499618.14		
15ESREGMAP01_04499618.26		
15ESREGMAP01_04499618.40		
15ESREGMAP01_04499618.52		
15ESREGMAP01_04499618.65		
15ESREGMAP01_04499618.79		
15ESREGMAP01_04499619.01		
15ESREGMAP01_04499619.13		
17ESAGENOR01_04666648.13	200 m	57°
17ESAGENOR01_04666649.52		
17ESAGENOR01_04666651.00		
17ESAGENOR01_04666652.39		
17ESAGENOR01_04666653.78		
17ESNERTRM01_04666645.52	230 m	81°
17ESNERTRM01_04666645.65		
17ESNERTRM01_04666645.78		
17ESNERTRM01_04666646.00		
17ESNERTRM01_04666646.13		
17ESNERTRM01_04666646.26		
17ESNERTRM01_04666646.39		
17ESNERTRM01_04666646.52		
17ESNERTRM01_04666646.65		
17ESREGMAP01_04666641.52	220 m	81°
17ESREGMAP01_04666641.65		
17ESREGMAP01_04666641.78		
17ESREGMAP01_04666642.00		
17ESREGMAP01_04666642.13		
17ESREGMAP01_04666642.26		
17ESREGMAP01_04666642.39		
17ESREGMAP01_04666642.52		
17ESREGMAP01_04666642.65		
17ESREGMAP01_04666642.78		
17ESREGMAP01_04666643.00		
17ESREGMAP01_04666643.13		
17ESREGMAP01_04666643.26		
17ESREGMAP01_04666643.39		
17ESREGMAP01_04666643.52		
17ESREGMAP01_04666643.65		
17ESREGMAP01_04666643.78		
17ESREGMAP01_04666644.00		
17ESREGMAP01_04666644.13		
19ESNORLAT01_04848847.00	200 m	78°
19ESNORLAT01_04848847.13		
19ESNORPLN01_04848882.07		
19ESNORPLN01_04848882.11		
19ESNORPLN01_04848882.42		
19ESNORPLN01_04848882.46		
19ESNORPLN01_04848882.49		
19ESNORPLN01_04848882.53		
19ESREGMAP01_04848845.00	200 m	78°
C3ESWEDGES01_03686394.00	420 m	87°

We followed the general principles of planetary mapping practices (Wilhelms, 1972, 1990; Skinner and Tanaka, 2003; Tanaka and others, 2005, 2011), including observation-based classification of geologic units (for example, units defined by color or texture). This method of classification helps to ensure that objective unit and feature descriptions are valid for any future Europa dataset. Interpretations are subject to change with time, especially with future, more detailed datasets anticipated from the Europa Clipper or other missions. However, we believe that this map will retain its relevance owing to the objective methods used in our mapping.

Geologic mapping started with authors Leonard and Patthoff each separately mapping a set of global unit boundaries, lineaments, and point features. The two independent maps were then compared and discussed. Leonard and Patthoff compromised when differences arose, such as the boundary locations and whether or not features should be included on the map. For areas where Leonard and Patthoff could not readily reach a compromise, author Senske provided a tiebreaking decision. This process of discussing each feature, point, and line ensures as much objectivity and consistency as possible across the map. Additionally, Senske reviewed the map at each stage to provide a third analysis of each boundary, lineament, and point feature. We feel the highest level of objectivity and consistency was reached by using this process.

The difference between geologic mapping of terrestrial planetary bodies and icy satellites is important. Geologic mapping of traditional planetary bodies often distinguishes between rock types; whereas, mapping on icy satellites such as Europa distinguishes between the morphologies of deformed and undeformed ice or non-ice materials. Units defined here are assumed to represent three-dimensional volumes of ice, each with a distinct relative brightness, texture, or unique structure. The actual depths of the units are unknown. We specifically note and emphasize that the morphologic differences between units could be due to a variety of factors, including compositional variation, tectonic deformation, or physical or chemical alteration by some other endogenic or exogenic process. This is in contrast to most geologic maps on Earth, which are primarily based on lithological differences.

Units

We identified only units of sufficient areal extent or geologic prominence to portray on the global geologic framework at 1:15,000,000 map scale. We defined requirements for unit mapping as follows: greater than 15 km wide for quasi-linear features (units cpr and b), greater than 50 km diameter for quasi-circular features (units chl, chm, chh, and chM) and regional plains material (unit pr), and greater than 10 km diameter for crater units (c, ce, and cpre). We assigned craters a smaller threshold than other units because of their rarity and importance in absolute age dating. We included linear features and point features on our map (see Location Features section), despite their smaller size, owing to their importance in understanding the geologic history of the surface. However, because of their limited local areal extent, we mapped these features with line or point symbols instead of as a separate unit (see Linear Features and Location Features sections).

Relative to earlier maps, this global map includes additional units and, therefore, additional colors. The units defined on this map are grouped by morphologic type and named with respect to that type (fig. 3, map sheet). This practice is commonly used for mapping on Europa (for example, Prockter and others, 1999; Figueredo and Greeley, 2004; Prockter and Schenk, 2005; Doggett and others, 2009). We also based unit names and colors on previously published maps of Europa to preserve the precedent and to make this map more easily comparable to other published maps of Europa (for example, Greeley and others, 2000; Figueredo and Greeley, 2000; Prockter and others, 2002; Doggett and others, 2009).

Contacts

Many contacts on this map are marked as as approximately located (long-dashed line) to show the location of gradual changes in surface-material characteristics. An approximate contact is common between the regional plains and chaos units. When mapping on higher resolution (tens to hundreds of m/px) images, certainty of the presence and location of unit boundaries is higher (for example, Prockter and Schenk, 2005; Leonard and others, 2018), which is often not the case at the global scale. We reserved the certain contact designation (solid line) for those units where we could identify a clear and distinct separation between units. Commonly, this occurs at the boundary between band units and adjacent units or around well-defined isolated chaos-unit occurrences, such as Murias Chaos (lat 22° N., long 273° E.). The clearly defined units that we mapped with a certain contact are generally only resolvable on the higher resolution images (<500 m/px) and are confined to the pole-to-pole mosaics on the leading and trailing hemispheres. We show an inferred contact (short-dashed line) where the presence of the contact is assumed because of the adjacent area of higher resolution image. This contact is used where the image resolution is low (greater than 2 km/px) but is adjacent to higher resolution imagery (fig. 2), where units are identified and assumed continuous. We show an inferred-questionable contact (queried short-dashed line) where the presence and location of the contact is uncertain, which is generally near the north and south poles, where image resolution and quality are the lowest. These questionable contacts are often in regions where the unit contact location is particularly uncertain owing to low resolution (>5 km/px) images or non-ideal imaging geometry. In these regions, contacts are based almost solely on relative brightness (texture is not resolvable).

Linear Features

Features less than ~15 km wide were too narrow to be resolvable or distinguished as units at the 1:15,000,000 map scale. However, we mapped some of these features, because of their width (>5 km), length (>hundreds of kilometers), or relative brightness compared to the surrounding terrain. We mapped these structures with a line feature, which marks the length, location, and trend of the feature. Typically, we used images with a resolution greater than ~250 m/px to discern ridges, troughs, band lineae, or other structures. Because of the low-resolution imaging

of much of Europa, we categorized many of the linear features as "undifferentiated linea" (see Undifferentiated Linea section). We intend for this nonspecific categorization to imply that these lineae could be any of the specified structures or possibly some other type of undescribed or unrecognized structure.

At image boundaries where a region has been resolved at both high and low resolutions, we classified the feature, when possible, to discern its morphological characteristics in the higher resolution images. When the structure could be traced into the lower resolution image, we then classified it as undifferentiated, because the defining characteristics were no longer resolvable. This results in a more conservative designation of the features. We chose this method because many linear features were observed to be composed of multiple types of structures along their length (for example, ridge and band linea). Therefore, we are unable to determine that a feature that appears as one structure on a higher resolution image continues to be that same type of structure farther along its length when imaged at a lower resolution.

Not all lineaments on Europa's surface are included on this map. The lineaments that we mapped are prominent (for example, distinctly longer and wider than most) and useful for constraining stratigraphy or aid in expressing the density and distribution of the other lineaments in the area. Lineaments that are distinct stratigraphic markers have a broad regional extent, especially those that bridge low-resolution areas or crosscut multiple units. They also have clear relative relations compared to other features or geologic units.

Location Features

We mapped features that were visible at 1:15,000,000 map scale but too small to be classified as units or linear features as location features or point features. These include microchaos, central peak structures, and small craters. The location features are mapped by placing a point near the center of the outcrop to identify its location. Outcrops of microchaoses mapped in the higher resolution images (<1 km/px) appear as small (<50 km diameter) occurrences of chaos material. The difference in these images between mapping chaos (unit) versus microchaos (point) was whether coalescence of the material was discernable at the 1:15,000,000 map scale. In the lower resolution images, we identified outcrops of microchaos as a quasi-circular region of low relative brightness and assumed these to be chaos material. Central peak structures and small craters are only identified where resolution is sufficient to clearly observe the shapes of these features (<1 km/px).

Limitations of Mapping and Recommendation for Use

We have taken care to maintain consistent mapping practices across the varying image viewing and lighting geometries (fig. 2) to capture as much detail as possible. This consistency is especially important where the relative brightness and texture of particular units can vary greatly owing to different viewing geometries. In this case, we define the unit using the most predominant appearance, consistent with the primary characteristics of the unit.

The range in resolution of images used to compile the mosaic has resulted in some regions being mapped with greater certainty and density of structures (such as leading and trailing hemispheres) than others (such as sub-Jovian and anti-Jovian hemispheres). In areas where only the lowest resolution images are available for the base mosaic (>2 km/px), we defined units based predominantly on apparent relative brightness rather than texture, as inferred by relative data number when compared to other regions containing the same unit (for example, fig. 4, map sheet). Additionally, in these low-resolution areas, individual structures are commonly not visible with the exception of a few wide (>20 km) linear features that have a distinct relative brightness contrast in relation to the background terrain.

When using this map, it is important to consider the following inherent bias owing to the varying resolution and imaging geometry:

1. The map is a representation of the surface, not a reproduction of the images. Therefore, we did not map every lineament, especially in regions of higher resolution (<250 m/px).

2. A conservative approach is taken when mapping continuous lineaments. If the authors have any doubt, the lineament is mapped as discontinuous. Additionally, linear features can change type along their length, causing the feature to appear discontinuous in GIS.

3. Units that we mapped in the lower resolution images (>2 km/px) are based on relative brightness and on data from neighboring, contiguous, higher resolution images.

Geologic Units

Four primary material-unit types were defined for this map: regional plains, bands, chaoses, and craters. We based these definitions and the naming scheme on previous maps of Europa, making changes as necessary to conform to the global resolution (Greeley and others, 1998, 2000; Senske and others, 1998; Prockter and others, 1999; Figueredo and Greeley, 2000, 2004; Prockter and Schenk, 2005; Doggett and others, 2009). Units are described below from oldest to youngest.

Regional Plains Material

Distributed over all latitudes and longitudes, regional plains material (unit pr) is the most pervasive unit on Europa (see table 2). It is characterized by a generally uniform high relative brightness compared to other terrain units and is predominately crosscut by all other units. At the global image scale, this unit appears smooth. However, when observed in higher resolution images (<250 m/px), a texture is revealed and small-scale (200–500 m in width) complex systems of subparallel to crosscutting ridges and troughs are apparent. In areas of low resolution (>1 km/px), the regional plains are either inferred from nearby higher resolution images or represent undivided terrain where other units cannot be identified. The

Table 2. Percentages of surface areas for four major unit and material types and for the microchaos point feature.

[%, percent; unit pr, regional plains material; unit chl, low-relative-brightness chaos material; unit chm, mottled chaos material; unit chh, high-relative-brightness chaos material; unit chM, Moytura chaos material; unit b, band material; unit c, crater material; unit ce, continuous crater-ejecta material; unit cpre, Pwyll radial crater-ejecta material; and unit cpr, Pwyll crater-ray material]

Unit and material	Areal coverage (%)
Regional plains (pr)	53.0
Chaos (chl, chm, chh, chM)	40.0
Bands (b)	3.5
Microchaos[1]	2.0
Crater (c, ce, cpre, cpr)	1.5

[1]Area of each microchaos (more than 2,300 points) is assumed to be the area of a circle with a radius of 10 kilometers. Microchaos is shown on the map as a point symbol (see Explanation of Map Symbols on map sheet).

type locality is lat 32° S., long 143° E. (fig. 3*A*). This unit is interpreted as a relatively old ice crust that has been deformed through multiple generations of tectonic processes.

Band Unit

Outcrops of band material (unit b) are defined by large linear to curvilinear landforms (>15 km in width and as much as hundreds of kilometers in length) with a range of relative brightness. The majority of band-material units have a lower relative brightness compared to the surrounding terrain; however, in limited places, some bands do appear to have a high relative brightness (see High-Relative-Brightness Band Linea section). This unit contains linear to curvilinear zones that have distinct boundaries defined by abrupt relative brightness and texture changes from the surrounding materials. The relative-brightness change with respect to the background terrain can be low or high and is not necessarily constant in images with varying incidence angles. For the band unit, we mapped only those that are greater than 15 km in width and at least 30 km in length. Shorter and narrower bands are also identified as linear features (see Band Linea section). In some regions where high-resolution imaging (<250 m/px) is available, bands can be subdivided as smooth, lineated, or ridged (Figueredo and Greeley, 2004; Prockter and Patterson, 2009) but, at the global scale, we group them together because of the limited extent of the high-resolution-image coverage. The type locality is lat 32° S., long 163° E. (fig. 3*B*).

In some locations, band materials are hypothesized to have formed by a process analogous to mid-ocean-ridge-style rifting and spreading, where a rift forms and the crustal blocks separate and spread laterally as new material rises at the spreading axis (for example, Prockter and others, 2002). This hypothesis is supported by plate reconstruction where, for some band material, separated landforms on either side of the band material can be accurately reconstructed when the band is closed. Recent work suggests that the varying morphologies of bands may be due to varying ice-shell rheologies and spreading rates (Howell and Pappalardo, 2018).

Chaos Units

Chaos material (units chM, chh, chm, chl), initially identified from data at the tens to hundreds of meters per pixel scale, generally consists of high-relative-brightness blocks of crustal material ranging from tens of meters to tens of kilometers in size. The blocks reside within a lower relative brightness hummocky matrix (Greeley and others, 2000; Doggett and others, 2009; Kattenhorn and Hurford, 2009). Chaos units are distinguished loosely based on relative brightness, which can be verified across incidence angle and resolution. Ideally, the distinction between chaos units would not be based on relative brightness alone but, at the lowest resolutions and incidence angles in the global mosaic, we must resort to this methodology for classification because no texture is discernible. As an aid to mitigate this lack of texture, we quantify the designation of high vs. low vs. mottled relative brightness using the relative data numbers of each unit (fig. 4, map sheet). The total area of chaos occupies approximately 40 percent of Europa's surface (table 2). Smaller occurrences of chaos, "microchaos," are identified as a location feature (see Location Features section).

The disrupted chaos terrain is inferred to be associated with a variety of potential formational hypotheses: where possible higher heat flow is found with respect to the surrounding terrain; where the subsurface ocean is in close proximity to the surface (Greenberg and others, 1999); where ice-shell convection results in upwelling (for example, Pappalardo and others, 1999b; Greeley and others, 2000); or where subsurface lakes have formed within the ice-shell (Schmidt and others, 2011). The lower relative brightness matrix material associated with chaos terrain typically has been interpreted to have a higher concentration of non-ice material and is inferred to have originated through interaction with the subsurface ocean (Shirley and others, 2010; Dalton and others, 2012).

Low-Relative-Brightness Chaos Material

Characterized by low-relative-brightness material with rounded blocks of regional plains (1 km to tens of kilometers) in a matrix with smooth patches on a 1 km to tens of kilometers scale or rough texture (containing blocks hundreds of meters to kilometers in scale), this material is named low-relative-brightness chaos material (unit chl). In higher resolution data, we observed that blocks can stand high or low with respect to the surrounding material. In areas of lower resolution (>1 km/px), this terrain appears smooth with low-relative-brightness material punctuated irregularly by small (kilometer-scale) areas of varying brightness. This unit primarily occurs on the anti-Jovian hemisphere, where radiation affects surface-material properties and sulfur is implanted from Io (for example, Dalton and others, 2013). The low relative brightness may be due to a high percentage of matrix material relative to the disrupted existing crustal blocks and (or) a high concentration of non-ice material and the effects of radiation on this material. The type locality is lat 1° S., long 105° E. (fig. 3*C*).

Mottled Chaos Material

We define mottled chaos material (chm) as disrupted terrain that contains outcrops of patchy (tens of kilometers scale) relative

bright to dark material. The unit contains rounded and angular blocks of regional plains material on a 1 km to tens of kilometers scale in a matrix with a smooth (1 km to tens of kilometers) or rough texture (containing blocks hundreds of meters to kilometers wide). The darkest materials (~10 km scale) are typically smooth on the kilometer scale. In areas of lower resolution (>1 km/px), this terrain has a high degree of mottling (tens of kilometers scale) with material of varying brightness. The type locality is lat 23° S., long 276° E. (fig. 3*D*). This unit abuts low-relative-brightness chaos material (unit chl) on the anti-Jovian hemisphere, possibly implying a genetic relation, but it also occurs over all latitudes and longitudes. The brightness variations may be caused by a nearly equal percentage of matrix material and disrupted pre-existing crustal blocks of regional plains material (unit pr) and (or) from variations in non-ice content. The patchy brightness could also result from the incomplete coalescence and consolidation of microchaos into a broader outcrop of chaos.

High-Relative-Brightness Chaos Material

Possessing a high-relative-brightness material compared to the surrounding terrain, high-relative-brightness chaos material (unit chh) contains tens-of-kilometers-scale angular blocks of regional plains material (unit pr) in a matrix with a rough texture (containing angular blocks hundreds of meters to kilometers in scale). In areas with lower resolution images (>1 km/px), this terrain appears smooth with high-relative-brightness material punctuated irregularly every ~10–100 km by small (kilometer scale) areas of low brightness. The type locality is lat 10° N., long 290° E. (fig. 3*E*). This unit occurs primarily on the sub-Jovian hemisphere, where a high degree of radiation processes of surface materials. The higher relative brightness may contain a low percentage of matrix material relative to the existing crustal blocks and (or) indicate a higher degree of radiation processing of the ice and, possibly, non-ice materials.

Moytura Chaos Material

Moytura chaos material (chM) is a unique morphology of chaos. It is composed of disrupted terrain that contains a smooth material (on a kilometer scale) that stands topographically higher than the surrounding terrain. The terrain is broken up by outcrops of regional plains material on an ~20–50 km scale and by curvilinear depressions. The type locality is lat 46° S., long 67° E. (fig. 3*F*). We only identify Moytura chaos material (unit chM) at one location on Europa, on the southern trailing hemisphere (lat 45° S., long 70° E. at an incidence angle >45°); however, this may be an observational bias caused by a lack of widespread images with a resolution of <500 m/px.

Crater Units

Craters and their associated ejecta deposits cover ~2 percent of Europa's surface (see table 2). On Europa, the transition between the impact crater and its ejecta is not commonly well defined and the crater rim can be difficult to discern, especially for some of the larger craters. The material units are defined based on their apparent morphology, brightness with respect to the background material, and relation to the central crater structure.

Crater Material

Crater material (unit c) is a quasi-circular depression with a raised rim or complex annular structure, such as multiple rings. Crater materials with a diameter greater than 10 km are mapped as units. Smaller craters (5–10 km diameter) are mapped as point features. Craters can also have little apparent topographic relief and (or) an association with an annular structure consisting of discontinuous ridges and troughs. The crater floor can range from generally flat to bowl-shaped and is interpreted to be controlled by the energy of the impacting event and age of the crater (Schenk, 2002). The unit includes material within the excavated area, which may represent impact melt, or subsequent infilling due to post-impact cryomagmatic processes (Moore and others, 1998, 2001; Schenk and others, 2004; Schenk and Turtle, 2009). Some craters contain blocks or other slumped material, and some craters contain a central peak structure. Because of the wide morphological variations among craters, Europa lacks a type example for crater material.

Continuous Crater-Ejecta Material

Continuous crater-ejecta material (unit ce) is made up of knobby terrain with rounded blocks and 100-m-scale roughness. This unit corresponds to the region found immediately surrounding craters and typically extending as far as ~5 crater radii from the crater material. In some cases, crater material has contrasting relative brightness to the background terrain. We interpret this to be material excavated during an impact and deposited proximally to the impact site. The type locality is lat 1° N., long 196° E. (fig. 3*G*).

Pwyll Radial Crater-Ejecta Material

Only found around Pwyll crater, the Pwyll radial crater-ejecta material (unit cpre) typically consists of a mottled brightness, where the high-relative-brightness material is radially distributed in quasi-linear broad streaks around the crater material (unit c). This material buries or subdues the underlying regional plains material (unit pr). Pwyll radial crater-ejecta material is interpreted to be formed by distal ejecta emplacement and secondary impact cratering (Bierhaus and others, 2001, 2009; Moore and others, 2001). This material is located ~5–10 crater radii away from unit c. The type locality is lat 25° S., long 79° E. (fig. 3*H*). The relatively pristine nature of the deposit suggests that Pwyll crater may be one of the youngest craters on Europa (Bierhaus and others, 2001).

Pwyll Crater Ray Material

Found at greater than 10 crater radii from the central crater material, Pwyll crater ray material (cpr) corresponds to isolated

high-relative-brightness patches. This unit is aligned quasi-linearly and distributed radially with respect to a central point (Pwyll crater). The type locality is lat 9° S., long 97° E. (fig. 3*I*). Unit cpr is found only around Pwyll. We interpret this unit to have formed through secondary impacts (Bierhaus and others, 2001, 2009; Moore and others, 2001).

Linear and Location Features

We identify linear features and location features on the basis of criteria outlined in the Linear Features and Location Features sections. Previously hypothesized formation mechanisms are outlined in this section. A type example for each linear feature can also be found in figure 3 (map sheet). We describe features below in approximate chronostratigraphic order from oldest to youngest.

Undifferentiated Linea

With a width greater than 5 km, undifferentiated lineae are long (tens to hundreds of kilometers), linear, through-going features of contrasting relative brightness, light or dark, and texture relative to the background terrain. These structures have no other discernible characteristics at the global scale or at any available image resolution. The type locality is lat 38° S., long 38° E. (fig. 3*J*). These lineae are most likely examples of troughs, ridges, subdued or brightened ridge complexes, or band lineae that are unclassifiable because of the limits of resolution and the viewing geometry constraints.

Ridge Linea

Ridge lineae, quasi-linear topographic highs that contain one or more crests, are identified in the image by a bright face perpendicular to the direction of the image lighting followed by a dark face. The type locality is lat 46° N., long 202° E. (fig. 3*K*). Ridge lineae are most commonly identified as double ridges (two ridges separated by a trough) or ridge complexes (more than two ridges separated by troughs) at higher resolution (for example, Greeley, 2000). The multiple types of morphologies suggest ridges could be formed through a variety of processes or represent different stages of the same process (Pappalardo and others, 1998). However, at the resolution of this map, differentiation among ridge types is not possible; therefore, we group all ridges into a single classification.

Band Linea

Band lineae are linear to curvilinear zones less than 15 km in width that contain an abrupt relative-brightness change compared to surrounding terrain. These features have the same or similar formation mechanism as band material (unit b), because they appear to have similar morphological characteristics but on a smaller scale (see Band Unit section). Portions of a band identified in band material (unit b) can be represented as a band linea for the segments where it is too narrow (>15 km) to be represented as a unit. The type locality is lat 34° S., long 177° E. (fig. 3*L*).

High-Relative-Brightness Band Linea

As opposed to band material, high-relative-brightness band lineae have an abrupt relative brightness increase, relative to the surrounding region, at all available incidence angles. We identify three such bands (Greenberg, 2004): two are located in the southern anti-Jovian hemisphere centered around lat 45° S., long 150° E.; the third is located at lat 16° N., long 334° E. The type locality is lat 41° S., long 147° E., (fig. 3*M*).

Cycloid

We define "cycloid" as a series of arcs connected by at least two sharp cusps (Greeley and others, 2000; Kattenhorn and Hurford, 2009). For our mapping, we require two cusps to define a cycloid, which ensures structures with just one cusp that do not form a series of arcs (for example, prominent lineament at lat 39° N., long 193° E.) are excluded from this classification. Additionally, the second cusp allows for a trend to be defined and a chain to become apparent, as described in Kattenhorn and Hurford (2009). This structure can have the morphology of a band or a ridge. In some instances, a single cycloid can appear to be composed of alternating segments of ridges and bands. The cycloidal shape suggests influence by a changing direction of crack propagation under the control of Europa's diurnally rotating stress field (Hoppa and others, 1999) or by tail-crack propagation (Marshall and Kattenhorn, 2005). The greatest concentrations of cycloids are centered primarily around 0° and 180° E. longitude. The type locality is lat 16° N., long 205° E. (fig. 3*N*).

Microchaos Material

Mapped as a point feature, microchaos material appears as circular to oblong, 10- to 75-km-diameter disruptions of the background terrain, which is predominately the regional plains material (unit pr; see Regional Plains Material section). Microchaos material has a lower relative brightness or different texture than the regional plains material (unit pr). The boundaries can be well defined when image resolutions are sufficient. However, on lower resolution images, the boundaries are less distinct. These features are also referred to as pits, domes, and spots (for example, Greeley and others, 2000); although, we find that it is not possible to distinguish amongst these structures at this map scale. We mapped approximately 2,300 of these features globally. The morphological similarities between microchaos (also referred to in the literature as "lenticulae") and larger chaos areas (see Chaos Units section) suggest a related formation process or variation of the same formation process (for example, Pappalardo and others, 1998). The type locality is lat 38° N., long 132° E. (fig. 3*S*).

Multi-Ring Structure

Found in proximity to some locations of crater material, multi-ring structures are identified by a quasi-circular to arcuate series of continuous or discontinuous ridges within a matrix of crater-ejecta material. At the global resolution, these structures are associated with a crater, Tegid (22 km diameter), and two large ringed features,

Tyre (62 km diameter) and Callanish (23 km diameter), which are interpreted to be impact craters (also noted in Schenk and Turtle, 2009). The type locality is lat 17° S., long 25° E. (fig. 3*O*). These quasi-concentric, multi-ring structures are interpreted as graben that formed by the collapse of an impact crater. The lack of other topography at these craters could be indicative of weak ice at depth within Europa's ice shell (Schenk, 2002).

Trough

Interpreted as quasi-linear, narrow (~5 km wide) topographic lows with material on either side showing no apparent offsets, troughs are identified by a dark-bright pairing perpendicular to the image lighting. We infer troughs to be local tension cracks, formed under extension. At the global resolution, these are only identified on the northern leading to sub-Jovian hemispheres. The type locality is lat 43° N., long 4° E. (fig. 3*P*).

Depression Margin

Depression margins are traces of broad, shallow topographic lows. Structures within the depressions appear undisrupted and well preserved. Some depression margins have well-defined walls while others are more subdued and have a gentle slope. Previous research suggests that these features might be indicative of geologically recent polar wander (Schenk and others, 2008). The type locality is lat 8° N., long 19° E. (fig. 3*Q*).

Central Peak Structure

A structure located near the center of some craters is mapped as the point feature named "central peak structure." This formation can appear as a simple peak or a complex structure. Eleven craters that have central peak structures are identified on this map. The type locality is lat 14° S., long 129° E. (fig. 3*R*).

Relative Ages

The relative ages of geologic units and structures on planetary bodies are determined largely by superposition, crosscutting, and embayment relations, as well as with crater statistics. The structure or unit that appears to be on top of, or deforming, another structure or unit is inferred to be younger. However, determining relative ages of structures or units on Europa is challenging for a variety of reasons including (1) the overall complexity of the surface, (2) the lack of consistent image resolution at the global scale necessary to determine crosscutting relations, and (3) the small number of impact craters for reliable crater statistics. Despite these limitations, we are able to draw general conclusions about the history of Europa's surface. Note that the dashed sides of the unit boxes and the dotted lines of the linear features in the Correlation of Map Units and Linear Features (map sheet) indicate uncertainty in the relative ages of the respective terrain or feature.

Surface Complexity

Europa is different from most other icy satellites, because it has a surface that is dominated by complex tectonic features and is geologically young (Zahnle and others, 1998, 2003). The complex surface can make it difficult to trace a single feature for long distances (tens to hundreds of kilometers), because the feature will be observed to cut across and be cut by numerous other features. Commonly, a structure will abruptly terminate or not be completely imaged. However, at the local scale, the use of crosscutting relations is ideal for determining relative ages, but projecting those relations to a global scale is hampered by the lack of available high-resolution images connecting the hemispheres.

Dating events by relative age is limited on Europa; for example, reactivation can occur. A specific example is shown in figure 5*A* (map sheet), where feature a is older than b, which in turn is older than c, but it appears that c is older than a, a relation that most likely involves reactivation of older tectonic features. This example, and others, commonly results in individual age relations that can be ambiguous. Recognizing this caveat to using superposition and crosscutting relations to obtain relative ages of any individual structure, we construct our stratigraphy on the basis of relations where the stratigraphy can be established with a high degree of confidence.

Image-Resolution and Illumination Geometry

As previously discussed, the variation in resolution and illumination geometry of the images making up the global mosaic can lead to challenges in mapping (fig. 5*B*). This especially affects determining relative ages when a structure or unit spans multiple images, which is common given the length and (or) extent of the linear features and geological units. In terms of illumination geometry, in particular incidence angle (fig. 2), this variation across the available images of the surface can lead to drastic relative-brightness changes at image boundaries when the incidence angle changes from high to low or vice versa. Additionally, structural and topographic relations, which can aid greatly in determining relative ages of crosscutting features or units, are subdued when the incidence angle is low. For many regions on Europa, potential discrepancies can be resolved and relative ages, especially for the larger structures mapped here, can be determined.

Paucity of Impact Craters

Typically, when determining the age of planetary surfaces, mappers look at crater density, size-frequency distributions, and other impact-crater characteristics that can inform relative age (for instance, degradation or relaxation) (for example, Collins and others, 2013; Tanaka and others, 2014). The young surface of Europa (Bierhaus and others, 2009) and the corresponding paucity of craters at the global scale creates limitations, because we cannot use crater-observation methods to aid in dating the various units. We have mapped only 47 craters on Europa's surface at the 1:15,000,000 scale. Too few craters are observed

on Europa to rely on statistical methods on how the distribution or degradation state might indicate age. Our reliance is primarily on crosscutting relations of structures and units to determine the relative relations of the geologic units, but we can, for example, use the crater Pwyll as a stratigraphic marker because its ejecta blanket is regionally widespread and forms distinct overlapping relations with other units.

Chronostratigraphy

We have determined chronostratigraphic history for Europa on the basis of superpositioning and cross cutting relationships among continuous map units (see Correlation of Map Units on map sheet). Uncertainty in stratigraphic relations is represented by the dashed edges and open ends of the unit-box boundaries and the dotted lines of the linear features. The three geologic periods are made equal length in the Correlation of Map Units because the actual relative lengths are unknown.

Europa's visible surface history of ~60–100 Ma may be divided into three general periods (Zahnle, 1998, 2003; Bierhaus and others, 2009). The first, or oldest, of these periods is dominated by the formation of the regional plains material (unit pr), ridges, and undifferentiated lineae, which indicates that this period was dominated by ridge-building processes. We make this interpretation because no older units or structures crosscut the regional plains material (unit pr). Ridges and undifferentiated lineae crosscut each other, but they do not appear to be younger than any other feature, structure, or unit at the global scale.

The second, or middle, period is dominated by the formation of band material (unit b), high-relative-brightness band material (unit chh), and undifferentiated lineae. Band material (unit b) generally appears younger and crosscuts the regional plains material (unit pr). Cycloids also appear to have formed during this period. Note that cycloids can appear similar to ridge or band-lineae structures and even transform from one to the other along their length, potentially indicating a transition from a ridge-building to a band-forming mechanism (for example, lat 0°, long 133° E.).

The third, or most recent, period is dominated by chaos-terrain formation, including the emplacement of microchaos. At the global scale, chaos terrain does not appear to be crosscut except by some craters and their ejecta; the troughs in the northern leading hemisphere; and, potentially, depression margins. Similarly, microchaos appears to have broken up previously formed bands, ridges, cycloids, and other features, which generally indicates that it is younger. However, we assume that each microchaos is formed relatively contemporaneously with one another, but they may have more realistically been emplaced over an extended period of time. Regardless, none of the microchaos are older than the regional plains material (unit pr). However, all of the features on the Correlation of Map Units and Linear Features (map sheet) extend to the present day in dashed form owing to uncertainty in crosscutting relations caused by the scale of the features.

Although we identified three periods in Europa's surface history, we emphasize that they are heavily intertwined with one another and are not necessarily discrete periods. For example, in most places across Europa, it is not clear how an instance of band material is related chronologically to an instance of low-relative-brightness chaos material when no observed crosscutting relations are visible between the two features. Thus, it remains uncertain whether every instance of low-relative-brightness chaos material is younger than every instance of band material, and in fact there may be considerable overlap in the ages of these features. Our resulting chronostratigraphy is consistent with the chronostratigraphy in published regional maps of Europa (for example, Greeley and others, 2000; Figueredo and Greeley, 2004).

Geologic Summary

The data provided by the Voyager and the Galileo missions has allowed significant insight to be established about the geological processes that have shaped or continue to shape the ice crust of Europa. Completion of a global map at a uniformly high resolution (tens to hundreds of meters per pixel) will need to wait for data from the Europa Clipper mission, now in development (Phillips and Pappalardo, 2014).

As a result of our global mapping of Europa, we find three general periods of resurfacing have taken place: the first and oldest period dominated by the formation of regional plains material (unit pr), the second period dominated by band (unit b) formation, and the third dominated by chaos (units chM, chh, chm, chl) formation. The oldest unit identified in this map, regional plains material, is also the most pervasive, covering >50 percent of Europa's surface (table 2). The bland appearance of the regional plains unit at the global scale is in stark contrast with the complex and intricate systems of subparallel to crosscutting ridges and troughs that are apparent at the regional scale in high-resolution images (<100 m/px).

Materials forming bands are subdivided into a unit and two linear features—band material (unit b), band linea, and high-relative-brightness band linea. The relative brightness within the high-relative-brightness band linea is consistent despite the change in incidence and emission angle; whereas, the brightness of the band material varies significantly, though the majority of bands appear to have a low relative brightness with respect to the surrounding terrain. The relative brightness variation of a specific band with changing incidence and emission angle could be due to grain size or macro-scale roughness, which implies that high-relative-brightness band lineae are potentially smoother or have smaller grains than band lineae or band material. Additionally, or alternatively, the relative brightness differences from band to band could indicate salt-concentration-radiation exposure or age (Lucchitta and Soderblom 1982; Schenk and McKinnon, 1989; Geissler and others, 1998; Carlson and others, 2002; Prockter and Patterson, 2009). Band material makes up 3.5 percent of Europa's surface area (table 2).

The chaos material is divided into four morphological categories that we differentiate based on texture and relative brightness: high-relative-brightness chaos material (unit chh), mottled chaos material (unit chm), low-relative-brightness chaos material (unit chl), and Moytura chaos material (unit chM). Although various hypotheses have been proposed to explain the formation of chaos, no consensus has been reached

on the mechanism for its emplacement (see Chaos section). The results of our mapping provide a quantitative assessment of the areal distribution of chaos terrain and its variability across Europa; all four chaos units cover ~40 percent of Europa's surface, and some outcrops extend laterally for hundreds to thousands of kilometers. Mapped occurrences of microchaos, summing to ~2 percent of the surface area (assuming an average area of 314 km^2 per microchaos feature, see table 2), are distributed across the surface and may have resulted from a similar process as chaos formation on the basis of their morphology and texture.

Impact craters and their associated deposits cover less than 2 percent of Europa's surface area. The crater material is divided into four morphological units: crater material (unit c), continuous crater-ejecta material (unit ce), Pwyll radial crater-ejecta material (unit cpre), and Pwyll crater-ray material (unit cpr). Units cpre and cpr are found only around Pwyll, potentially one of the youngest craters on Europa (Bierhaus and others, 2001). The overall paucity of impact craters—we map 47 in total—suggests Europa has a geologically youthful surface.

In addition to the geologic units, we have mapped structural features that include depression margin, trough, multi-ring structure, cycloid, band linea, ridge, and undifferentiated linea. We have mapped more than 2,300 occurrences of microchaos as point features along with two other point features of craters, small craters (<10 km diameter), and central peak structures. Because of their great extent (hundreds of kilometers), the linear features are significant stratigraphic markers that we used to establish global-scale crosscutting relations and are essential to understanding the global geologic history of Europa.

Depression margins appear to be some of the youngest features on Europa's surface, because they appear not to be disrupted by the interior terrain. Troughs are also relatively young structures on Europa's surface, because no other features appear to crosscut them, except for limited associations with chaos terrain. The same also applies to multi-ring structures identified as the large ringed features, Callanish and Tyre, and a crater, Tegid. Cycloids extend across Europa's surface over as much as hundreds of kilometers and can vary in relative age. Band lineae have the same relative age as the band material (unit b). Ridges typically occur within the regional plain material (unit pr) and are crosscut by the chaos material units (units chh, chm, chl, and chk), microchaos, craters, and other linear features. Undifferentiated lineae could potentially consist of ridges, band lineae, or other structures and are often unresolvable, so their potential age is widely uncertain and could span much of Europa's surface history.

On the basis of the identifiable crosscutting relations between the map units and linear features, this global geologic map reveals three relatively distinct periods in Europa's surface history. With this map, we have analyzed and summarized the state of knowledge on Europa's geological history. The apparent need for resurfacing mechanisms to create Europa's current young surface is made especially clear through the lack of craters and the wide variety of units and features identified on our map. However, much of the surface will likely remain a mystery until additional imaging and compositional data become available through the Europa Clipper mission, which is currently set to launch in October 2024.

Acknowledgments

We thank Robert Pappalardo (Jet Propulsion Laboratory, California Institute of Technology), Jim Skinner (U.S. Geological Survey [USGS]), and Corey Fortezzo (USGS) for useful discussions throughout the course of this work. Marc Hunter (USGS) was instrumental with setting up the GIS project that was used for this mapping. We also thank Geoffrey Collins (Wheaton College) for supplying the high-resolution mosaic. We acknowledge Melissa Bunte (Arizona State University) and Thomas Doggett (Arizona State University) for their previous work on this map and Jose Pablo Brenes Coto (Wheaton College) for creating the image mosaic in figure 1*B*. We also thank three anonymous reviewers for their helpful insights for this work. This work was supported by the Furukawa Memorial Fellowship at the University of California, Los Angeles (UCLA) and by the National Aeronautics and Space Administration (NASA) headquarters under the NASA Earth and Space Science Fellowship Program, Grant 80NSSC17K0602. This project was also supported by the Europa Clipper Project. Portions of this research were carried out at the Jet Propulsion Laboratory, California Institute of Technology, under contract with NASA. This map would not have been published without the incredible work of Dr. Ronald Greeley, who originally led this effort and was always an advocate for geologic mapping.

References Cited

Anderson, J.D., Schubert, G., Jacobson, A., Lau, E.L., Moore, W.B., and Sjogen, W.L., 1998, Europa's differentiated internal structure—Inferences from four Galileo encounters: Science, v. 281, p. 2019–2022, https://www.science.org/doi/10.1126/science.281.5385.2019.

Batson, R.M., 1987, Digital cartography of the planets—New methods, its status, and its future: Photogrammetric Engineering and Remote Sensing, v. 53, p. 1211–1218.

Becker, T.L., Archinal, B., Colvin, T.R., Davies, M.E., Gitlin, A., Kirk, R.L., and Weller, L., 2001, Final digital global maps of Ganymede, Europa, and Callisto: Lunar and Planetary Science XXXII, abstract 2009.

Becker, T.L, Rosanova, T., Cook, D., Davies, M.E., Colvin, T.R., Acton, C., Bachman, N., Kirk, R.L., and Gaddis, L.R., 1999, Progress in improvement of geodetic control and production of final image mosaics for Callisto and Ganymede: Lunar and Planetary Science XXX, abstract 1692.

Becker, T.L., Rosanova, T., Gaddis, L.R., McEwen, A.S., Phillips, C.B., Davies, M.E., and Colvin, T.R., 1998, Cartographic processing of the Galileo SSI data—An update on the production of global mosaics of the Galilean satellites: Lunar and Planetary Science XXIX, abstract 1892.

Bierhaus, E.B., Chapman, C.R., Merline, W.J., Brooks, S.M., and Asphaug, E., 2001, Pwyll secondaries and other small craters on Europa: Icarus, v. 153, p. 264–276, https://doi.org/10.1006/icar.2001.6690.

Bierhaus, E.B., Zahnle, K., and Chapman, C.R., 2009, Europa's crater distributions and surface ages, *in* Pappalardo, R.T., McKinnon, W.B., and Khurana, K.K, eds., Europa: Tucson, University of Arizona Press, p. 161–180.

Bunte, M.K., Greeley, R., Doggett, T., Figueredo, P., Tanaka, K., and Senske, D., 2013, Finalization of the global geologic map of Europa: Lunar and Planetary Science XLIV, abstract 1719.

Carlson, R.W., Anderson, M.S., Johnson, R.E., Schulman, M.B., and Yavrouian, A.H., 2002, Sulfuric acid production on Europa—The radiolysis of sulfur in water ice: Icarus, v. 157, p. 456–463.

Cassen, P.M., Peale, S.J., and Reynolds, R.T., 1982, Structure and thermal evolution of the Galilean satellites, *in* Morrison, D., ed., Satellites of Jupiter: Tucson, University of Arizona Press, p. 93–128.

Cassen, P.M., Reynolds, R.T., and Peale, S.J., 1979, Is there liquid water on Europa?: Geophysical Research Letters, v. 6, p. 731–734, https://doi.org/10.1029/GL006i009p00731.

Collins, G.C., Patterson, G.W., Head, J.W., Pappalardo, R.T., Prockter, L.M., Lucchitta, B.K., and Kay, J.P., 2013, Global geologic map of Ganymede: U.S. Geological Survey Scientific Investigation Map 3237, scale 1:15,000,000.

Cooper, J.F., Johnson, R.E., Mauk, B.H., Garrett, H.B., and Gehrels, N., 2001, Energetic ion and electron irradiation of the icy Galilean satellites: Icarus, v. 149, no. 1, p. 133–159, https://doi.org/10.1006/icar.2000.6498.

Dalton, J.B., III, Cassidy, T., Paranicas, C., Shirley, J.H., Prockter, L.M., and Kamp, L.W., 2013, Exogenic controls on sulfuric acid hydrate production at the surface of Europa: Planetary and Space Science, v. 77, p. 45–63, https://doi.org/10.1016/j.pss.2012.05.013.

Dalton, J.B., Shirley, J.H., and Kamp, L.W., 2012, Europa's icy bright plains and dark linea—Exogenic and endogenic contributions to composition and surface properties: Journal of Geophysical Research, v. 117, 16 p., https://doi.org/10.1029/2011JE003909.

Danielson, G.E., Kupferman, P.N., Johnson, T.V., and Soderblom, L.A., 1981, Radiometric performance of the Voyager cameras: Journal of Geophysical Research, Space Physics, v. 86, no. 10, p. 8683–8689, https://doi.org/10.1029/JA086iA10p08683.

Davies, M.E., Abalakin, V.K., Bursa, M., Lieske, J.H., Morando, B., Morrison, D., Seidelmann, P.K., Sinclair, A.T., Yallop, B., and Tjuflin, Y.S., 1995, Report of the IAU/IAG/COSPAR Working Group on Cartographic Coordinates and Rotational Elements of the Planets and Satellites—1994: Celestial Mechanics and Dynamical Astronomy, v. 63, p. 127–148, https://doi.org/10.1007/BF00693410.

Davies, M.E., Colvin, T.R., Oberst, J., Zeitler, W., Schuster, P., Neukum, G., McEwen, A.S., Phillips, C.B., Thomas, P.C., Veverka, J., Belton, M.J.S., and Schubert, G., 1998, The control networks of the Galilean satellites and implications for global shape: Icarus, v. 135, p. 372–376, https://doi.org/10.1006/icar.1998.5982.

Davies, M.E., and Katayama, F.Y., 1981, Coordinates of features on the Galilean Satellites: Journal of Geophysical Research, v. 86, p. 8635–8657, https://doi.org/10.1029/JA086iA10p08635.

Doggett, T., Greeley, R., Figueredo, P., and Tanaka, K., 2009, Geologic stratigraphy and evolution of Europa's surface, *in* Pappalardo, R.T., McKinnon, W.B., and Khurana, K.K, eds., Europa: Tucson, University of Arizona Press, p. 137.

Eliason, E.M., 1997, Production of digital image models using the ISIS system: Lunar and Planetary Science XXVIII, p. 331.

Figueredo, P.H., Chuang, F.C., Rathbun, J., Kirk, R.L., and Greeley, R., 2002, Geology and origin of Europa's "Mitten" feature (Murias Chaos): Journal of Geophysical Research, v. 107, 15 p., https://doi.org/10.1029/2001JE001591.

Figueredo, P.H., and Greeley, R., 2000, Geologic mapping of the northern leading hemisphere of Europa from Galileo solid-state imaging data: Journal of Geophysical Research, v. 105, p. 22629–22646, https://doi.org/10.1029/1999JE001107.

Figueredo, P.H., and Greeley, R., 2004, Resurfacing history of Europa from pole-to-pole geological mapping: Icarus, v. 167, p. 287–312, https://doi.org/10.1016/j.icarus.2003.09.016.

Gaddis, L.R., Anderson, J., Becker, K., Becker, T.L., Cook, D., Edwards, K., Eliason, E.M., Hare, T., Kieffer, H.H., Lee, E.M., Mathews, J., Soderblom, L.A., Sucharski, T., Torson, J., McEwen, A.S., and Robinson, M., 1997, An overview of the Integrated Software for Imaging Spectrometers (ISIS): Lunar and Planetary Science XXVIII, p. 387.

Geissler, P., Greenberg, R., Hoppa, G., McEwen, A., Tufts, R., Phillips, C., Clark, B., Ockert-Bell, M., Helfenstein, P., Burns, J., Veverka, J., Sullivan, R., Greeley, R., Pappalardo, R.T., Head, J.W., Belton, M.J.S., Denk, T., and the Galileo Imaging Team, 1998, Evolution of lineaments on Europa—Clues from Galileo multispectral imaging observations: Icarus, v. 135, p. 107–126, https://doi.org/10.1006/icar.1998.5980.

Greeley, R., and Batson, R.M., 1990, Planetary mapping: Cambridge, UK, Cambridge University Press, 396 p.

Greeley, R., Figueredo, P.H., Williams, D.A., Chuang, F.C., Klemaszewski, J.E., Kadel, S.D., Prockter, L.M., Pappalardo, R.T., Head, J.W., III, Collins, G.C., Spaun, N.A., Sullivan, R.J., Moore, J.M., Senske, D.A., Tufts, B.R., Johnson, T.V., Belton, M.J.S., and Tanaka, K.L., 2000, Geologic mapping of Europa: Journal of Geophysical Research, v. 105, p. 22559–22578, https://doi.org/10.1029/1999JE001173.

Greeley, R., Sullivan, R., Klemaszewski, J., Homan, K., Head, J.W., III, Pappalardo, R.T., Veverka, J., Clark, B.E., Johnson, T.V., Klaasen, K.P., Belton, M., Moore, J., Asphaug, E., Carr, M.H., Neukum, G., Drek, T., Chapman, C.R., Pilcher, C.B., Geissler, P.E., Greenberg, R., and Tufts, R., 1998, Europa—Initial Galileo geologic observations: Icarus, v. 135, p. 4–24, https://doi.org/10.1006/icar.1998.5969.

Greenberg, R., 2004, The evil twin of Agenor—Tectonic convergence on Europa: Icarus, v. 167, p. 313–319, https://doi.org/10.1016/j.icarus.2003.09.025.

Greenberg, R., Hoppa, G.V., Tufts, B.R., Geissler, P., Riley, J., and Kadel, S., 1999, Chaos on Europa: Icarus, v. 141, p. 263–286, https://doi.org/10.1006/icar.1999.6187.

Hand, K.P., Chyba, C.F., Priscu, J.C., Carlson, R.W., and Nealson, K.H., 2009, Astrobiology and the potential for life on Europa, *in* Pappalardo, R.T., McKinnon, W.B., and Khurana, K.K, eds., Europa: Tucson, University of Arizona Press, p. 589–629.

Head, J.W., Sherman, N.D., Pappalardo, R.T., Thomas, C., Greeley, R., and the Galileo SSI team, 1998, Cryovolcanism on Europa—Evidence for the emplacement of flows and related deposits in the E4 region (5N, 305W) and interpreted eruption conditions: Lunar and Planetary Science Conference XXIX, abstract 1491.

Hoppa, G.V., Tufts, B.R., Greenberg, R., and Geissler, P.E., 1999, Formation of cycloidal features on Europa: Science, v. 285, p. 1899–1902, https://www.science.org/doi/full/10.1126/science.285.5435.1899.

Howell, S.M., and Pappalardo, R.T., 2018, Band formation and ocean-surface interaction on Europa and Ganymede: Geophysical Research Letters, v. 45, no. 10, p. 4701–4709, https://doi.org/10.1029/2018GL077594.

Kadel, S.D., Chuang, F.C., Greeley, R., Moore, J.C., and the Galileo SSI team, 2000, Geologic history of the Tyre region of Europa—A regional perspective on Europan surface features and ice thickness: Journal of Geophysical Research, v. 105, p. 22657–22669, https://doi.org/10.1029/1999JE001203.

Kargel, J.S., Kaye, J.Z., Head, J.W.I., Marion, G.M., Sassen, R., Ballesteros, O.P., Grant, S.A., and Hogenboom, D.L., 2000, Europa's crust and ocean—Origin, composition, and the prospects for life: Icarus, v. 148, p. 226–265, https://doi.org/10.1006/icar.2000.6471.

Kattenhorn, S.A., 2002, Nonsynchronous rotation evidence and fracture history in the bright plains region, Europa: Icarus, v. 157, p. 490–506, https://doi.org/10.1006/icar.2002.6825.

Kattenhorn, S.A., and Hurford, T., 2009, Tectonics of Europa, *in*, Pappalardo, R.T., McKinnon, W.B., and Khurana, K.K, eds, Europa: Tucson, University of Arizona Press, p. 199–236.

Kirk, R.L., Thompson, K.T., Becker, T.L., and Lee, E.M., 2000, Photometric modeling for planetary cartography: Lunar and Planetary Science XXXI, abstract 2025.

Kivelson, M.G., Khurana, K.K., Russell, C.T., Volwerk, M., Walker, R.J., and Zimmer, C., 2000, Galileo magnetometer measurements—A stronger case for a subsurface ocean at Europa: Science, v. 289, p. 1340–1343, https://www.science.org/doi/10.1126/science.289.5483.1340.

Klemaszewski, J.E., Greeley, R., Prockter, L.M., Geissler, P.E., and the Galileo SSI team, 1999, Geologic mapping of eastern Agenor Linea, Europa: Lunar and Planetary Science Conference XXX, abstract 1680.

Leonard, E.J., Pappalardo, R.T., and Yin, A., 2018, Analysis of very-high-resolution Galileo images and implications for resurfacing mechanisms on Europa: Icarus, v. 312, p. 100–120, https://doi.org/10.1016/j.icarus.2018.04.016.

Lucchitta, B.K., and Soderblom, L.A., 1982, The geology of Europa, *in* Morrison, D., ed., Satellites of Jupiter: Tucson, University of Arizona Press, p. 521–555.

Marshall, S.T., and Kattenhorn, S.A., 2005, A revised model for cycloid growth mechanics on Europa—Evidence from surface morphologies and geometries: Icarus, v. 177, p. 341–366, https://doi.org/10.1016/j.icarus.2005.02.022.

McCord, T.B., Hansen, G.B., Matson, D.L., Johnson, T.V., Crowley, J.K., Fanale, F.P., Carlson, R.W., Smythe, W.D., Martin, P.D., Hibbitts, C.A., Granahan, J.C., and Ocampo, A., 1999, Hydrated salt minerals on Europa's surface from the Galileo near-infrared mapping spectrometer (NIMS) investigation: Journal of Geophysical Research, Planets, v. 104, no. E5, p. 11827–11851, https://doi.org/10.1029/1999JE900005.

McEwen, A.S., 1991, Photometric functions for photoclinometry and other applications: Icarus, v. 92, p. 298–311, https://doi.org/10.1016/0019-1035(91)90053-V.

Moore, J.M., Asphaug, E., Belton, M.J., Bierhaus, B., Breneman, H.H., Brooks, S.M., Chapman, C.R., Chuang, F.C., Collins, G.C., Giese, B., Greeley, R., Head, J.W., Kadel, S., Klaasen, K.P., Klemaszewski, J.E., Magee, K.P., Moreau, J., Morrison, D., Neukum, G., Pappalardo, R.T., Phillips, C.B., Schenk, P.M., Senske, D.A., Sullivan, R.J., Turtle, E.P., and Williams, K.K., 2001, Impact features on Europa—Results of the Galileo Europa Mission (GEM): Icarus, v. 151, no. 1, p. 93–111, https://doi.org/10.1006/icar.2000.6558.

Moore, J.M., Asphaug, E., Sullivan, R.J., Klemaszewski, J.E., Bender, K.C., Greeley, R., Geissler, P.E., McEwen, A.S., Turtle, E.P., Phillips, C.B., Tufts, R.B., Head, J.W., Pappalardo, R.T., Jones, K.B., Chapman, C.R., Belton, M.J.S., Kirk, R.L., and Morrison, D., 1998, Large impact features on Europa—Results of the Galileo nominal mission: Icarus, v. 135, p. 127–145, https://doi.org/10.1006/icar.1998.5973.

Nimmo, F., and Manga, M., 2009, Geodynamics of Europa's ice shell, *in* Pappalardo, R.T., McKinnon, W.B., and Khurana, K.K, eds., Europa: Tucson, University of Arizona Press, p. 381–404.

Pappalardo, R.T., Belton, M.J.S., Breneman, H.H., Carr, M.H., Chapman, C.R., Collins, G.C., Denk, T., Fagents, S., Geissler, P.E., Giese, B., Greeley, R., Greenberg, R., Head, J.W., Helfenstein, P., Hoppa, G., Kadel, S.D., Klaasen, K.P., Klemaszewski, J.E., Magee, K., McEwen, A.S., Moore, J.M., Moore, W.B., Neukum, G., Phillips, C.B., Prockter, L.M., Schubert, G., Senske, D.A., Sullivan, R.J., Tufts, B.R., Turtle, E.P., Wagner, R., and Williams, K.K., 1999b, Does Europa have a subsurface ocean? Evaluation of the geological evidence: Journal of Geophysical Research, v. 104, p. 24015–24055, https://doi.org/10.1029/1998JE000628.

Pappalardo, R.T., Head, J.W., and Greeley, R., 1999a, The hidden ocean of Europa: Scientific American, v. 281, no. 4, p. 54–63, https://www.jstor.org/stable/26058439.

Pappalardo, R.T., Head, J.W., Greeley, R., Sullivan, R.J., Pilcher, C., Schubert, G., Moore, W.B., Carr, M.H., Moore, J.M., Belton, M.J.S., and Goldsby, D.L. 1998, Geological evidence for solid-state convection in Europa's ice shell: Nature, v. 391, p. 365–368, https://doi.org/10.1038/34862.

Phillips, C.B., and Korth, H., 2017, Choice of coordinate systems for planetary mapping by the Europa Clipper Project: Presentation given at the Europa Clipper System Convention, August 3, 2017, https://sbn.psi.edu/mc-f2f/2017/presentations/Europa%20Clipper%20Coordinate%20System%20Convention%2020170803.pdf.

Phillips, C.B., and Pappalardo, R.T., 2014, Europa Clipper mission concept—Exploring Jupiter's ocean moon: Eos Transaction of the American Geophysical Union, v. 95, no. 20, p. 165.

Prockter, L.M., Antman, A., Pappalardo, R.T., Head, J.W., and Collins, G.C., 1999, Europa—Stratigraphy and geologic history of an anti-Jovian region from Galileo E14 solid-state imaging data: Journal of Geophysical Research, v. 104, p. 16531–16540, https://doi.org/10.1029/1998JE001015.

Prockter, L.M., Head, J.W., Pappalardo, R.T., Sullivan, R.J., Clifton, A.E., Giese, B., Wagner, R., and Neukum, G., 2002, Morphology of Europan bands at high resolution—A mid-ocean ridge-type rift mechanism: Journal of Geophysical Research, v. 107, https://doi.org/10.1029/2000JE001458.

Prockter, L., and Patterson, G.W., 2009, Morphology and evolution of Europa's ridges and bands, *in* Pappalardo, R.T., McKinnon, W.B., and Khurana, K.K, eds., Europa: Tucson, University of Arizona Press, p. 237–258.

Prockter, L.M., and Schenk, P.M., 2002, Mapping of Europa's youthful dark spot—A potential landing site: Lunar and Planetary Science XXXIII, abstract 1732.

Prockter, L.M, and Schenk, P.M., 2005, Origin and evolution of Castalia Macula, an anomalous young depression on Europa: Icarus, v. 177, p. 305–326, https://doi.org/10.1016/j.icarus.2005.08.003.

Prockter, L.M., Shirley, J.H., Dalton, J.B., III, and Kamp, L., 2017, Surface composition of pull-apart bands in Argadnel Regio, Europa—Evidence of localized cryovolcanic resurfacing during basin formation: Icarus, v. 285, p. 27–42, https://doi.org/10.1016/j.icarus.2016.11.024.

Rhoden, A.R., Mohr, K.J., Hurford, T.A., Henning, W., Sajous, S., Patthoff, D.A., and Dubois, D., 2021, Obliquity, precession, and fracture mechanics—Implications of Europa's global cycloid population: Journal of Geophysical Research, Planets, v. 126, no. 3, https://doi.org/10.1029/2020JE006710.

Schenk, P.M., 2002, Thickness constraints on the icy shells of the Galilean satellites from a comparison of crater shapes: Nature, v. 417, p. 419–421, https://doi.org/10.1038/417419a.

Schenk, P.M., Chapman, C.R., Zahnle, K., and Moore, J.M., 2004, Ages and interiors—The cratering record of the Galilean satellites, *in* Bagenal, F., Dowling, T.E., and McKinnon, W.B., eds., Jupiter—The planet, satellites, and magnetosphere: Cambridge, UK, Cambridge University Press, p. 427–456.

Schenk, P.M., Matsuyama, I., and Nimmo, F., 2008, True polar wander on Europa from global-scale small-circle depressions: Nature, v. 453, p. 368–371, https://doi.org/10.1038/nature06911.

Schenk, P.M., and McKinnon, W.B., 1989, Fault offsets and lateral crustal movement on Europa—Evidence for a mobile ice shell: Icarus, v. 79, p. 75–100, https://doi.org/10.1016/0019-1035(89)90109-7.

Schenk, P.M., and Turtle, E.P., 2009, Europa's impact craters—Probes of the icy shell, *in* Pappalardo, R.T., McKinnon, W.B., and Khurana, K.K, eds., Europa: Tucson, University of Arizona Press, p. 181–198.

Schmidt, B.E., Blankenship, D.D., Patterson, G.W., and Schenk, P.M., 2011, Active formation of 'chaos terrain' over shallow subsurface water on Europa: Nature, v. 479, no. 7374, p. 502–505, https://doi.org/10.1038/nature10608.

Schubert, G., Sohl, F., and Hussmann, H., 2009, Interior of Europa, *in* Pappalardo, R.T., McKinnon, W.B., and Khurana, K.K, eds., Europa: Tucson, University of Arizona Press, p. 353–368.

Senske, D.A., Greeley, R., Head, J., Pappalardo, R., Sullivan, R., Carr, M., Geissler, P., Moore, J., and the Galileo SSI team, 1998, Geologic mapping of Europa—Unit identification and stratigraphy at global and local scales: Lunar and Planetary Science Conference IXXX, abstract 1743.

Shirley, J.H., Dalton, J.B., Prockter, L.M., and Kamp, L.W., 2010, Europa's ridged plains and smooth albedo plains—Distinctive compositions and compositional gradients at the leading side-trailing side boundary: Icarus, v. 210, p. 358–384, https://doi.org/10.1016/j.icarus.2010.06.018.

Skinner, J.A., and Tanaka, K.L., 2003, How should planetary map units be defined?: Lunar and Planetary Science Conference XXXIV, abstract 2100.

Smith, B.A., Briggs, G.A., Danielson, G.E., Cook, A.F., Davies, M.E., Hunt, G.E., Masursky, H., Soderblom, L.A., Owen, T.C., Sagan, C., and Suomi, V.E., 1977, Voyager imaging experiment: Space Science Reviews, v. 21, p. 103–127, https://doi.org/10.1007/BF00200847.

Spaun, N.A., Head, J.W., Collins, G.C., Prockter, L.M., and Pappalardo, R.T., 1998a, Conamara Chaos region, Europa—Reconstruction of mobile polygonal ice blocks: Geophysical Research Letters, v. 25, p. 4277–4280, https://doi.org/10.1029/1998GL900176.

Spaun, N.A., Head, J.W., Pappalardo, R.T., and the Galileo Imaging Team, 1998b, Geologic history, surface morphology and deformation sequence in an area near Conamara Chaos, Europa: Lunar and Planetary Science Conference XXIX, abstract 1899.

Sullivan, R., Greeley, R., Klemaszewski, J., Moreau, J., Head, J.W., Pappalardo, R.T., Moore, J., and Tufts, J.R., 1999, High resolution Galileo geologic mapping of ridges and plains on Europa: Lunar and Planetary Science Conference XXX, abstract 1925.

Tanaka, K.L., Robbins, S.J., Fortezzo, C.M., Skinner, J.A., and Hare, T.M., 2014, The digital global geologic map of Mars—Chronostratigraphic ages, topographic and crater morphologic characteristics, and updated resurfacing history: Planetary and Space Science, v. 95, p. 11–24, https://doi.org/10.1016/j.pss.2013.03.006.

Tanaka, K.L., Skinner, J.A., Jr., and Hare, T.M., 2005, Geologic map of the northern plains of Mars: U.S. Geological Survey Scientific Investigations Map 2888, 1 sheet, scale 1:15,000,000, 27-p. pamphlet.

Tanaka, K.L., Skinner, J.A., and Hare, T.M., 2011, Planetary geologic mapping handbook—2011: U.S. Geological Survey, Astrogeology Science Center, unpublished handbook, https://astropedia.astrogeology.usgs.gov/download/Docs/Mappers/PGM_Handbook_2011.pdf.

Torson, J.M., and Becker, K.J., 1997, ISIS—A software architecture for processing planetary images: Lunar and Planetary Science XXVIII, p. 1443.

Trumbo, S.K., Brown, M.E., and Hand, K.P., 2019, Sodium chloride on the surface of Europa: Science Advances, v. 5, no. no. 6, 4 p., https://doi.org/10.1126/sciadv.aaw7123.

U.S. Geological Survey, 2002, Controlled photomosaic map of Europa, Je 15M CMN: U.S. Geological Survey Geologic Investigations Series I–2757, https://pubs.usgs.gov/imap/i2757/.

Vance, S., and Goodman, J., 2009, Oceanography of an ice-covered moon, *in*, Pappalardo, R.T., McKinnon, W.B., and Khurana, K.K, eds., Europa: Tucson, University of Arizona Press, p. 459–482.

Wackett, L.P., Dodge, A.G., and Ellis, L.B.M., 2004, Microbial genomics and the periodic table: Applied and Environmental Microbiology, v. 70, p. 647–655, https://doi.org/10.1128/AEM.70.2.647-655.2004.

Wilhelms, D.E., 1972, Geologic mapping of the second planet: unpublished U.S. Geological Survey Interagency Report, Astrogeology 55, https://www.lpi.usra.edu/resources/USGS-Reports/Astro-0055.pdf.

Wilhelms, D.E., 1990, Geologic mapping, *in* Greeley, R., and Batson, R.M., eds., Planetary mapping: Cambridge, UK, Cambridge University Press, p. 208–260.

Williams, D.A., Klemaszewski, J.E., Greeley, R., Moore, J.M., Pappalardo, R.T., Prockter, L.M., Head, J.W., Geissler, P.E., Hoppa, G.V., Phillips, C.B., Tufts, B.R., Greenberg, R., Sullivan, R.J., Belton, M.J.S., and the Galileo Imaging Team, 1998, Terrain variation on Europa—Overview of Galileo Orbit E17 imaging results: Lunar and Planetary Science Conference XXX, abstract 1396.

Zahnle, K., Dones, L., and Levinson, H.F., 1998, Cratering rates on the Galilean satellites: Icarus, v. 136, p. 202–222, https://doi.org/10.1006/icar.1998.6015.

Zahnle, K., Schenk, P., Levinson, H., and Dones, L., 2003, Cratering rates in the outer solar system: Icarus, v. 163, p. 263–289, https://doi.org/10.1016/S0019-1035(03)00048-4.

Zolotov, M.Y., and Kargel, J.S., 2009, On the chemical composition of Europa's icy shell, ocean, and underlying rocks, *in* Pappalardo, R.T., McKinnon, W.B., and Khurana, K.K, eds., Europa: Tucson, University of Arizona Press, p. 431.